Optical and Vibrational Studies on Single Walled Carbon Nanotubes/Short Oligo-Para-Methoxy-Toluene Composite

A. Haj Said,[1] S. Ayachi,[2] I. Chefia,[1] J. Wéry,[3] K. Alimi[2]

[1]*Laboratoire Polymères, Biopolymères, Matériaux Organiques, Faculté des sciences, Université de Monastir, 5000, Tunisie*
[2]*Unité de Recherche, Matériaux Nouveaux et Dispositifs Electroniques Organiques, Faculté des Sciences, Université de Monastir, 5000 Monastir, Tunisie*
[3]*Institut des Matériaux Jean Rouxel, Nantes Atlantic Universites, 2 rue de la Houssinière, B.P. 32229, 44322 Nantes, Cédex 03, France*

Received 7 May 2010; accepted 2 February 2011
DOI 10.1002/app.34287
Published online 10 June 2011 in Wiley Online Library (wileyonlinelibrary.com).

ABSTRACT: In a solution state, an oligophenylene prepared by electrochemical oxidation of *para*-methoxy-toluene exhibited luminescence in the violet-to-blue region. However, in a solid state, a clear red shift was observed as a signature of a supramolecular π-stacking interaction between oligomer chains. In a de-doped state, by chemical reduction, a fine structure in the form of two peaks was observed and luminescence intensity was strongly improved. When mixed with single walled carbon nanotubes (SWNTs), a quenching in the luminescence intensity accompanied by a slight blue shift of the PL peak of the nanocomposite was observed. This implies the shortening of the oligomer's effective π-conjugation length caused by the added amount of SWNTs. A charge transfer in the photo-excited state was also noted. The interaction taking place between the two materials was supported by optical infrared absorption and Raman scattering measurements and then a functionalizing mechanism was proposed. © 2011 Wiley Periodicals, Inc. J Appl Polym Sci 122: 1889–1897, 2011

Key words: carbon nanotube; composites; infrared spectroscopy; π-stacking; photoluminescence

INTRODUCTION

Conventional polymer materials were traditionally used in applications such as packaging, electrical insulators, and photo-resists. However, new opportunities have emerged with the discovery of conducting polymers in 1977.[1] Since then, the dream of combining the polymers' mechanical and processing properties with the metals' electronic and optical properties has been the driving force of the science and technology related to conjugated conducting polymers.[2–4] Although these materials play a fundamental role in transistors, integrated circuits,[5,6] photovoltaic devices,[7,8] and light emitting devices,[9,10] it has become quite clear that the synthesis of well-defined conjugated polymers should lead to a significant improvement in the performance of these polymeric materials. Therefore, in an attempt to bring more reliable synthetic procedures to the field of electronic materials, a variety of synthetic tools were utilized, which allowed significant advances in this research field and the discovery of new and interesting conjugated structures.[11–13] Lately, the interest in conjugated oligomers has grown rapidly because of their good processability and semiconducting properties which were comparable with those of parent polymers.[14,15] In addition, these oligomers are used as model compounds for conducting polymers since their monodispersity, defectless structure, and their better supramolecular organization in the solid state facilitate experimental and theoretical investigations.[16,17]

The recent rise of nanotechnology has led to many reports on the synthesis and applications of nano-structured conducting polymers such as nanofibers and carbon nanotubes.[18,19] In this context, new methods of nano-structured polymer and polymer nanocomposite synthesis and characterization, as well as recent knowledge about their structure and properties are of fundamental interest.[20,21] Carbon nanotubes, and particularly single wall carbon nanotubes (SWNTs), are excellent reinforcing materials for a variety of matrices.[22,23] Thus, the synthesis and investigation of composites based on conducting polymeric matrices containing carbon nanotubes are currently very popular topics in the field of materials science and are being considered of theoretical and practical interest.[24,25] Polymer/CNT composites are expected to have the good processability

Correspondence to: A. Kamel (kamel.alimi@fsm.rnu.tn).
Contract grant sponsor: Tunisian-French cooperative action; contract grant number: CMCU/07G1309.

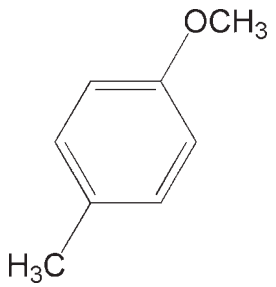

Scheme 1 Chemical structure of *para*-methoxy-toluene (PMT) monomer.

characteristics of the polymer and the excellent functional properties of the CNTs.[26,27] However, a homogeneous, uniform dispersion of the nanotubes in the polymer matrix, with significant interactions between them, is desirable in creating an optimal nanocomposite. This is a serious problem that inhibits their uniform incorporation into polymer matrices for the fabrication of advanced composite materials.

In this work, we report a detailed spectroscopic investigation that sheds light onto the interaction between the single walled carbon nanotube (SWNT) and the short length of luminescent oligomers obtained from electrochemical oxidation of *p*-methoxy-toluene (PMT). For this purpose, we develop various experimental methods including optical absorption, photoluminescence, infrared, and Raman scattering.

EXPERIMENTAL

Chemicals

Para-methoxy-toluene (Scheme 1) was provided by ACROS. The single-walled carbon nanotubes (SWNTs) powder used to prepare the composite (diameter: 1.2-1.5 nm, length: 2-5 μm, density: 1.7-1.9 g/mL) and the solvents such as chloroform ($CHCl_3$) and chlorobenzene (C_6H_5Cl) (used without further purification) were supplied by Sigma-Aldrich.

Electro-synthesis of oligo-para-methoxy-toluene (OPMT)

The oligomer electro-synthesis was detailed elsewhere.[28] Gavanostatic electrolyses (I = 300 mA) were carried out on 5 g of the starting material (C = 0.4*M*) in a nonseparated cell. The working electrode was a 16 cm^2 platinum grid and the counter electrode a 4 cm^2 platinum grid. The potentiostat and the current integrator were Tacussel, PRT 1-100, and IG-5*N*, respectively. During electro-synthesis, the electrolysis cell was immersed in an ultrasonic Bransonic 220 bath (48 kHz) to ensure solution stirring. To keep the ultrasonic bath at ambient temperature, water was regularly changed during electrolysis. The electrolysis solutions were extracted with chloroform. Then the polymer was precipitated successively in methanol, diethyl ether, and finally in cyclohexane. Our study is focused on the shorter-chain oligomer precipitated in cyclohexane. The average polymerization degree is about 9 and the polydispersity index is 1.4 as determined by the gel permeation chromatography analysis.[28] To de-dope the electro-synthesized material, we chemically reduced stabilized radical cations obtained by the overoxidation process taking place during electrosynthesis. Then, 0.5 g of oligomer, and 2 g of zinc dust were refluxed in THF for 6h.

SWNTs/OPMT composite preparation

The single walled carbon nanotubes (SWNTs), used in this study, were produced by the electric-arc technique. The SWNTS powder (1.6 mg) was added to 16 mL of chlorobenzene and the mixture was sonicated for 60 min at room temperature to disperse the carbon nanotubes. The choice of chlorobenzene as solvent was justified by its better ability to disperse SWCNTs than chloroform.[29] The short oligo(*p*-methoxy-toluene) (OPMT), in its doped state, was dissolved in the same solvent (chlorobenzene) (1.6 mg of OPMT in 1 mL of solvent). After mixing the appropriate quantity of the dispersed SWNTs (1 mL) with 1 mL of the oligomer solution (1.6 mg), a homogeneous, uniform dispersion of the nanotubes was obtained in the oligomer matrix with a 9% mass ratio (with respect to the starting composition). Subsequently, the obtained composite was carefully subjected to an ultrasonic process in an aqueous ultrasonication bath for 1 h.

Instruments and measurements

The instruments used for this work included thermogravimetric analysis (TGA) and differential thermal analysis (DTA), Fourier transform infrared (FT-IR), Raman scattering, photoluminescence, and optical absorption. The dynamic thermogravimetric analysis was carried out in a Perkin–Elmer TGS-1 thermal balance with a Perkin–Elmer UV-1 temperature program control. The samples were placed in a platinum sample holder, and the thermal degradation measurements were carried out between 300 and 973 K at a 5 K/min speed rate under air atmosphere.

Infrared absorption measurements were recorded using a Nicolet FTIR interferometer 20 SXC with a 4 cm^{-1} energy resolution. The samples, in solid state, were pellets of KBr mixed with the organic compound under study and the band positions were expressed in wave-number (cm^{-1}) from 400 to 2000. Raman scattering spectra were recorded using an excitation laser wavelength of 1064 nm on a Fourier

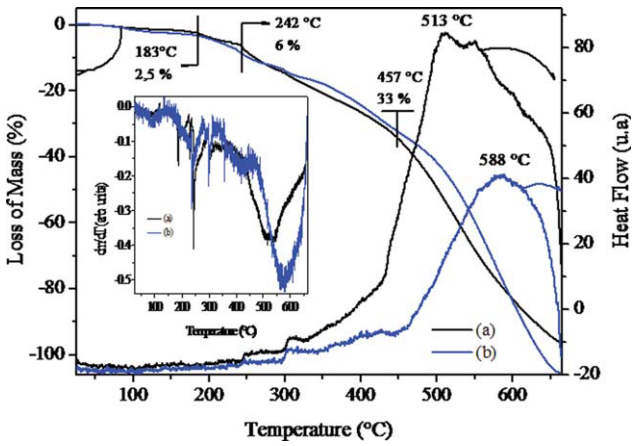

Figure 1 Thermogravimetric analysis (TGA) and differential thermal analysis (DTA) as well as the TGA first derivative curves of: (a) de-doped and (b) doped OPMT samples. [Color figure can be viewed in the online issue, which is available at wileyonlinelibrary.com.]

transform Raman spectrometer Bruker RFS 100, with a 4 cm^{-1} spectral resolution.

Optical absorption spectra were recorded using a Varian cary 5 UV-visible-near-infrared spectrometer. The wavelengths, expressed in nanometers for optical density, varied from 200 nm (6.2 eV) to 2000 nm (0.62 eV). Photoluminescence spectra were collected from the front-face geometry of the samples with a Jobin-Yvon Fluorolog spectrometer using a xenon lamp (500 W) as an excitation source. All experiments were carried out in ambient air at room temperature. The PL spectra measurements were performed using a wavelength excitation of 325 and 350 nm for solution and solid states, respectively.

RESULTS AND DISCUSSION

OPMT thermal and luminescence properties

Thermal analysis

Thermogravimetric analysis (TGA) and differential thermal analysis (DTA) were used to study the oligomer's thermal degradation in its doped and de-doped states. The obtained results are shown in Figure 1. First, we noted that oligomers had nearly the same thermal behaviors. Second, two fast degradations were found: the first occurred from 242 to 457°C with a maximum 33% weight loss, and the second fastest degradation starting from 457°C. It should be noted that a small weight loss (6%) from 183 to 442°C was observed, most probably related to evaporation of the residual solvents used during oligomer preparation and purification. The lower oligomers' heat-resistance as compared to PPP[30] can be explained by the presence of methyl/methoxy side chains, which are well known as vulnerable to elevated temperatures. Finally, the polyphenylene backbone degradation was started from 457°C as described in the literature.[30] The TGA first derivative curve, plotted in the same figure, supported the above assumption by the presence of two pronounced peaks indicating the side chains and the phenylene backbone degradations.

From the DTA curves, at least three exothermic peaks can be observed: the first at $\sim$ 245°C and the second at $\sim$ 306°C with a weaker intensity. This means that the first degradation is a simple chemical reaction and could be related to a separate departure of substituent groups. The third peak, the most relevant exothermic one, appeared at about 513 and 588°C for the de-doped and doped oligomers, respectively. The broadening of the exothermic peaks indicates that several reactions were occurring simultaneously.

Emission properties

The normalized room temperature photoluminescence spectrum of the studied material, in its doped state, in chloroform reveals a light emission in the violet-to-blue region (Fig. 2). Two broad peaks were located at 373 and 455 nm, as shown in Figure 2(b). However, when the spectrum was recorded for OPMT in solid state, only the red-shifted peak (446 nm) was observed [Fig. 2(a)]. This behavior is a signature of a supramolecular π-stacking interaction between oligomer chains in solution or solid states. It results from the π-π interactions between aromatic rings in adjacent chains leading to the packing of the conjugated segments.[31,32] Under these conditions, the broad and unstructured red-shifted emission can be attributed to excimers formed by the collision of

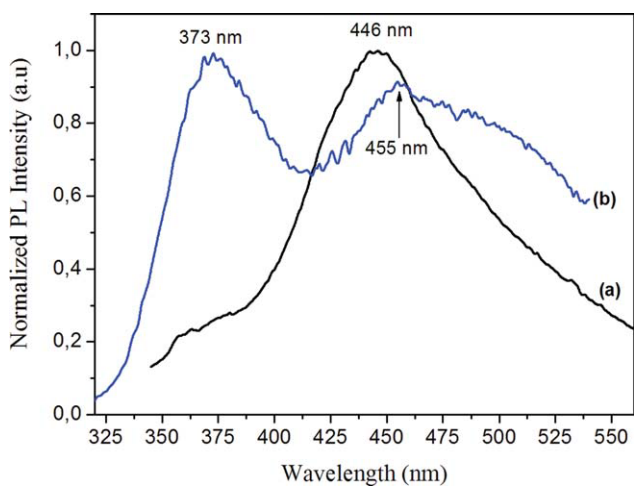

Figure 2 Normalized PL intensity spectra of doped OPMT: (a) in solid and (b) in chloroform solution states. [Color figure can be viewed in the online issue, which is available at wileyonlinelibrary.com.]

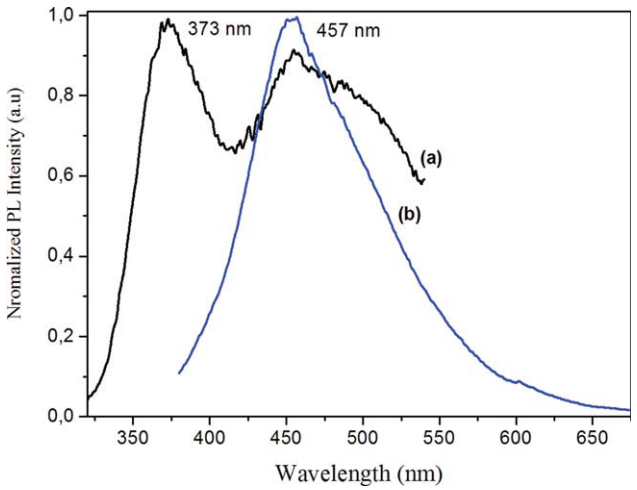

Figure 3 Normalized PL intensity spectra of doped OPMT in solution states: (a) chloroform and (b) chlorobenzene. [Color figure can be viewed in the online issue, which is available at wileyonlinelibrary.com.]

an electronically excited molecule with a molecule in the ground state.[33] The tendency of oligomer to self organize via π-π stacking seems to be enhanced in chlorobenzene (Fig. 3). This may be the consequence of the solvent's aromatic structure which facilitates the oligomer organization and even stakes with polyphenylene backbone. This phenomenon is accentuated in the solid state probably leading to more organized structures. Therefore, luminescence and charge transport properties will be seriously affected and exciton diffusion will be enhanced by interchain conjugation.

In addition, we have studied the effect of OPMT de-doping on its optical response. In fact, it is well known that de-doping electrochemically *p*-doped material can be achieved by chemical reduction.[34] For this purpose, we used zinc dust. The photoluminescence spectra, in solid state, were reported in Figure 4. For the OPMT de-doped state, two well-resolved peaks are detected at 424 and 447 nm, as a fine structure [Fig. 4(b)]. Moreover, for the OPMT doped state [Fig. 4(a)], we note only the presence of the peak centered at ~ 446 nm related to the oligomer's intrinsic properties. This band is usually assigned to the 0-0 electronic transition, while the second feature appearing at about 424 nm for the de-doped sample is attributed to the 0-1 electronic transition. This latter was totally suppressed in the doped form. Indeed, the presence of polarons species in the doped state induces the presence of intermediate electronic levels between the HOMO and the LUMO levels. As a result, a larger signal was obtained in the photoluminescence response [Fig. 4(a)]. Quantitatively, we note that the PL relative intensity ($\frac{I_{PL(de-doped)}}{I_{PL(doped)}} \approx 63$) was the evident signature of a quenching effect of the luminescence intensity in the doped state. Compared with the doped OPMT, a similar result was obtained for the de-doped state in chloroform [Fig. 5(A)]. Additionally, we decomposed the PL spectrum of the de-doped OPMT powder [Fig. 5(B)] with Lorentzian functions. Although deconvolution is always an arbitrary procedure, we define the dependence in position (λ: wavelength), line width (W), and integrated intensity (A) of PL peaks. As a result, the PL spectrum presents three characteristic peaks. For convenience,[35] we assigned the three vibronic peaks to 0-0 (1), 0-1 (2), and 0-2 (3) electronic transitions. Then, the highest transition energy is the 0-0 transition, which takes place between the zero vibronic level in both excited and ground states. The 0-1 and 0-2 transitions involve the creation of one phonon and replica phonons, respectively.

The study of the OPMT/SWNTs composite

Optical absorption and emission properties

In this section, we will present the optical and vibrational characterization of a nanocomposite elaborated from the OPMT and SWCNTs. This study has been spurred by the need to seek for new physical properties induced by the CNT insertion in the oligomer matrix. The nanocomposite was prepared as previously mentioned in the experimental section.

First, we compared in Figure 6 the UV-vis spectra of the doped OPMT and composite in chlorobenzene solution at room temperature. These spectra indicated that materials absorb in the UV region. Moreover, the UV-vis spectra [Fig. 6(A)] showed a three-shouldered spectra with maximums situated at around 271, 265, and 259 nm, which are noted as (1), (2), and (3), respectively. These peaks should be logically assigned to the transition of the vibronic structures (0-0, 0-1, and 0-2).[36] Therefore, the intensity of the three bands which are assigned to the transition

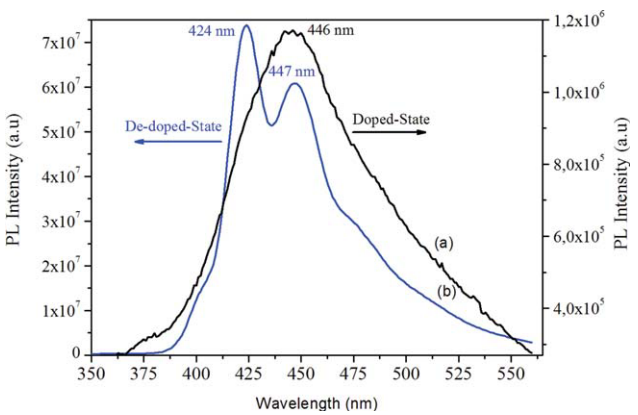

Figure 4 PL spectra of OPMT powder: (a) doped and (b) de-doped states. [Color figure can be viewed in the online issue, which is available at wileyonlinelibrary.com.]

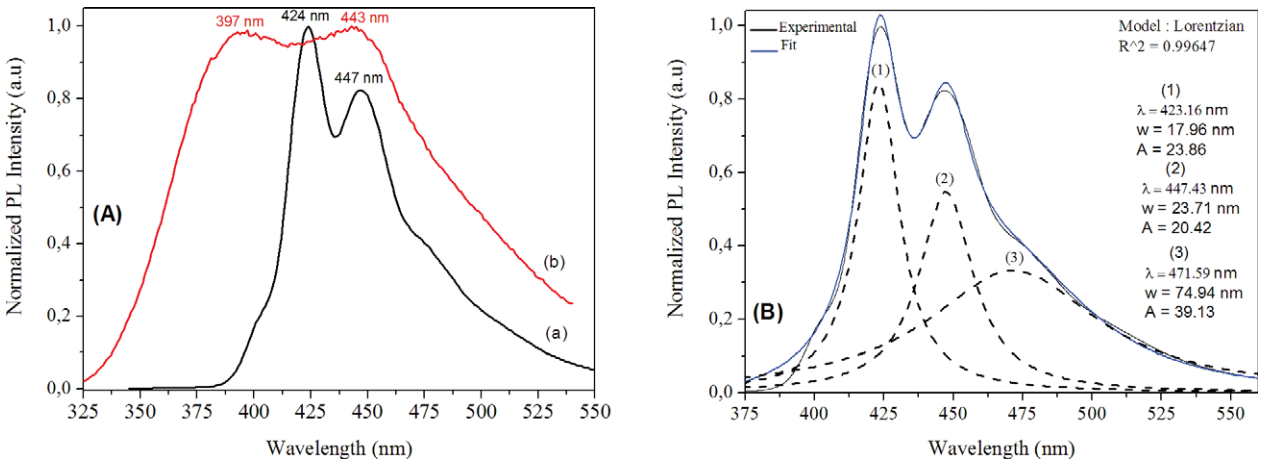

Figure 5 (A): Normalized PL Intensity spectra of de-doped OPMT: (a) in solid and (b) in chloroform solution states and (B): Normalized PL intensity spectrum decomposition of de-doped OPMT powder. W and A represent the line width and the integrated intensity, respectively. [Color figure can be viewed in the online issue, which is available at wileyonlinelibrary.com.]

between the localized and delocalized π orbital and π→π* transitions of π-electron states delocalized along the polymer chain were enhanced in the case of composite.[37,38] This is probably a proof of the shortening of the oligomer's segments. Compared to the doped oligomer, the optical band gap energy estimated from the extrapolation of the linear part of the optical absorption of the composite was reduced by 0.02 eV [Fig. 6(B)]. The estimated band gap energy (∼ 4.43 eV) is relatively higher than that of the PPP film (3.02 eV).[33] This higher band gap could be due to the presence of substituents on the phenyl ring, provoking a distorted conformation, on the one hand and to the low conjugation length along oligomer chains on the other.

Furthermore, UV-vis spectra can be deconvoluted (Fig. 7) with Gaussian functions. Accordingly and compared to the pristine sample [Fig. 7(a)], a slight red-shift of the composite's absorption peaks was observed, as indicted in Figure 7(b). The little changes concerning the main peak positions were probably related to the ground state interaction taking place between the two materials, and, thus, a little charge transfer occurs in the ground state.[39,40]

Likewise, we have studied the elaborated material's photoluminescence (Fig. 8). When the doped oligomer and composite (OPMT/SWNTs) solutions were excited, they emitted luminescence in the range 380–660 nm with a maximum at 444 and 457 nm, respectively. It was noteworthy that there was a clear decrease in the luminescence intensity ($\frac{I_{PL(oligomer)}}{I_{PL(composite)}} \approx 1.98$) (Fig. 8). The oligomer's normalized PL spectra and their corresponding composite are depicted in the beginning of Figure 8. In the blend, the slight blue shift (from 457 to 444 nm) of the PL peak is due to the shortening of the effective π-

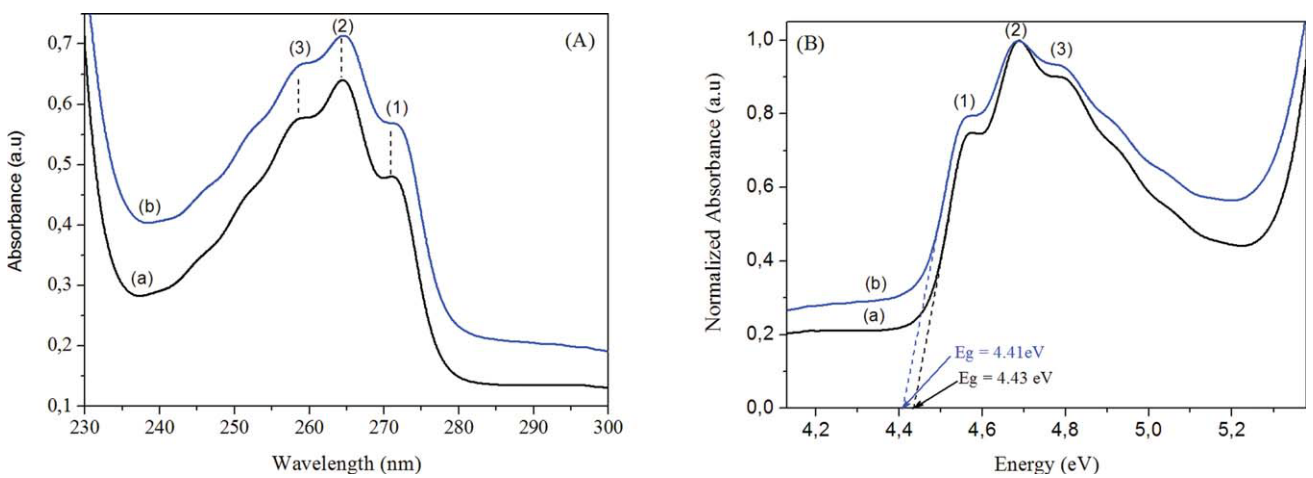

Figure 6 (A) Optical absorption spectra of (a) oligomer and (b) composite and (B) Normalized optical absorbance of (a) oligomer and (b) composite. [Color figure can be viewed in the online issue, which is available at wileyonlinelibrary.com.]

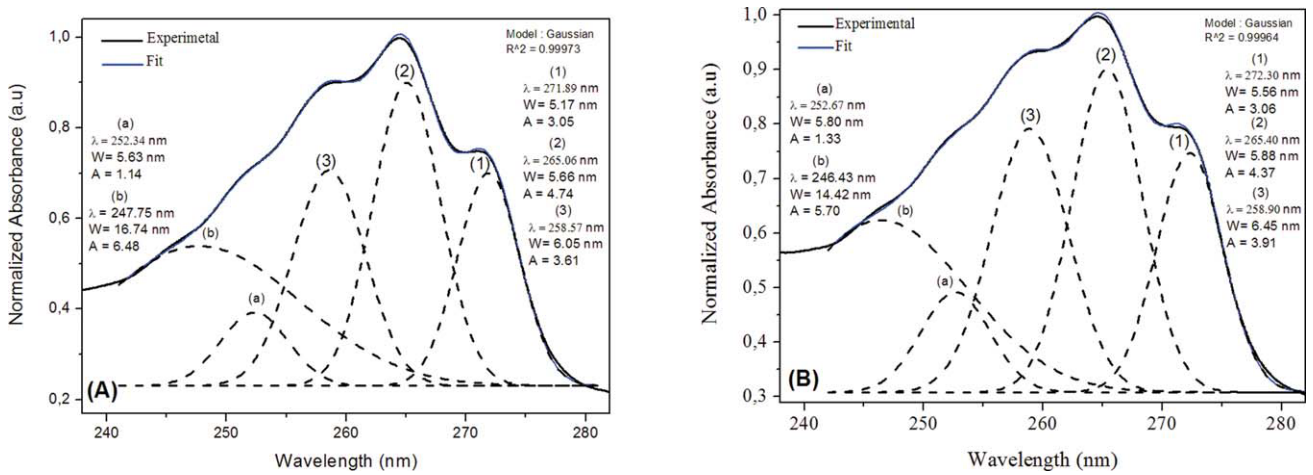

Figure 7 Normalized optical absorption spectra decomposition of: (a) oligomer and (b) composite. W and A represent the line width and the integrated intensity, respectively. [Color figure can be viewed in the online issue, which is available at wileyonlinelibrary.com.]

conjugation length attributed to the nanotubes presence, as reported in other works.[41] As a result, the luminescence quenching of the composite was ascribed to the absorption of the recombination energy by SWNTs, indicating that excitons generated in the oligomer were diminished before the radiative recombination due to the SWNTs presence.[42] This implies that a charge transfer from the photo-excited OPMT to the nanotube is expected to occur.

Vibrational properties: Infrared and Raman scattering measurements

Figure 9 displays normalized optical infrared spectra of OPMT, SWNTs, as well as the OPMT/SWNTs composite. In fact, according to Ref. 43 infrared absorbance bands for the SWNTs are observed at 1170, 1456, 1540, and 1734 cm^{-1}. In our case, these bands appear at 1174, 1440, 1579, and 1710 cm^{-1}, respectively. Furthermore, the peak at 1629 cm^{-1}, in the FTIR spectrum of SWNTs [Fig. 9(b)] indicates the presence of significant carbonyl groups in SWNTs as supplied.[44] Compared to the pristine oligomer [Fig. 9(a)], the infrared absorption spectrum of the composite [Fig. 9(c)] reveals significant changes. Considering the polymer CNTs' ratio in the composite, the CNT bands are expected to considerably lose their contribution to the composite's infrared spectra. Unlike the oligomer's characteristic broadened bands, the composite's absorption bands were sharp. Moreover, the absorption medium intensity band at 858 cm^{-1}, typical of a C—H out-of-plane vibration for tetra-substituted benzenes,[45,46] completely faded out. However, the intensities of peaks at 1365 and 1380 cm^{-1}, attributed to methyl stretching,[45,46] were considerably increased. Besides, the oligomer infrared absorption bands at 1463 and 1500 cm^{-1} attributed to aromatic ring stretching were dramatically changed.[45,46] The former was significantly reduced whereas the latter completely disappeared. Furthermore, two pronounced bands appeared at 1712 and 1764 cm^{-1}. They probably correspond to bands appearing at 1610 and 1652 cm^{-1} in the pristine oligomer that shifted to higher frequencies. These bands were assigned to the quinoid structure and carbonyl groups, respectively. In fact, the quinoid structure appeared as a result of electron subtraction by electrochemical doping[47] (see *vide infra* in Scheme 2). However, carbonyl groups can be described as a synthesis defect due to residual water attack on radical cation intermediates competitively with coupling reactions.[48] The whole vibrational results supported a strong oligomer-SWNTs' interaction. Actually, some bonds were loosened whereas other vibrations were hindered when passing from pristine oligomer to the composite.

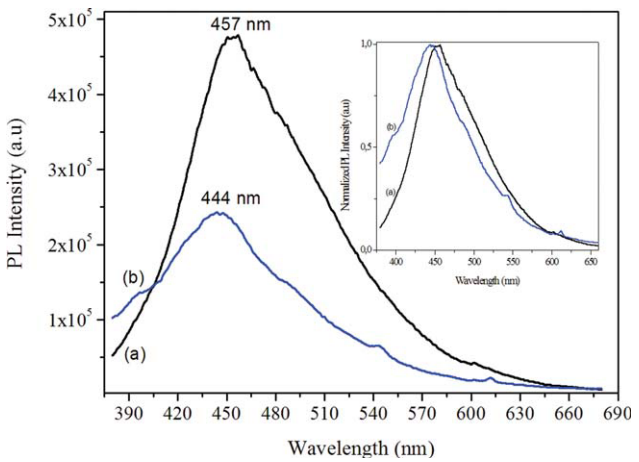

Figure 8 PL spectra of (a) oligomer and (b) composite. [Color figure can be viewed in the online issue, which is available at wileyonlinelibrary.com.]

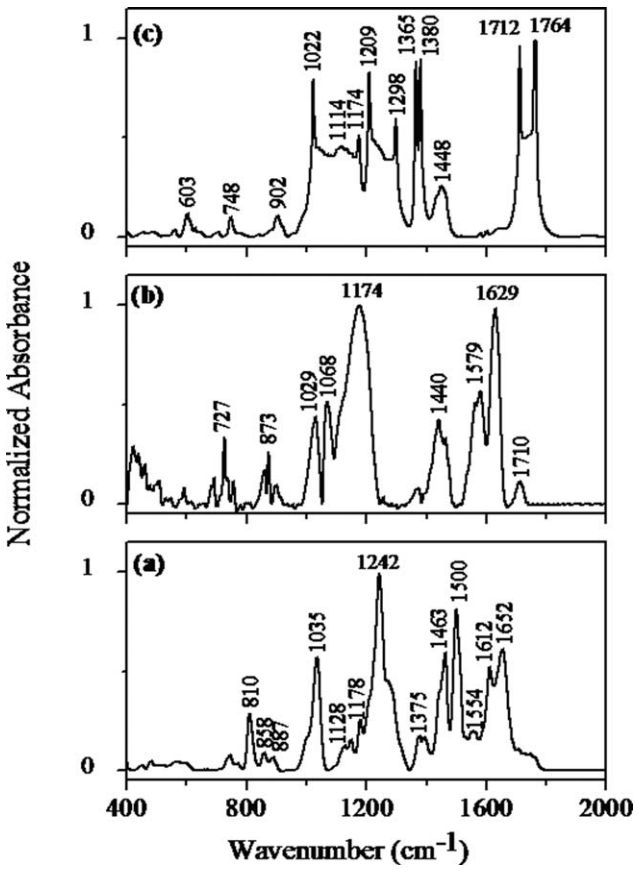

Figure 9 Normalized optical infrared spectra of (a) OPMT, (b) SWNTs, as well as the (c) OPMT/SWNTs composite.

Raman spectra recorded for the composite showed a well resolved spectrum compared to that of the oligomer which hardly diffuses light (Fig. 10). Compared to the SWNTs' Raman spectrum [Fig. 10(b)], it was clear that at least some modifications are noted, in the case of the composite. For the SWNTs and in the range 1100–1700 cm^{-1}, there are two bands: the first (1275 cm^{-1}), labeled "D band," is attributed to the disorder or defects on SWNTS, and the second (1593 cm^{-1}) is associated to tangential mode (TM) vibrations.[49] Previous experimental and theoretical studies have shown that doping SWNTs with either electron donors or acceptors or electrochemically resulted in noticeable shifts in certain characteristic vibrational modes.[50,51] Particularly, the observed downshift in the G band around 1592 cm^{-1} is related to the weakened C—C bond strength. In our case, by adding SWNTs, the down-shift of TM (from 1593 to 1574 cm^{-1}) (Fig. 10), which is logically attributed to the C=C stretching mode, decreases in intensity. This provides further evidence of the strong CNTs/oligomer interaction.

To appreciate the interaction within the OPMT/SWNTs composite, Figure 11 illustrates the radial breathing mode (RBM) features (in the first range:

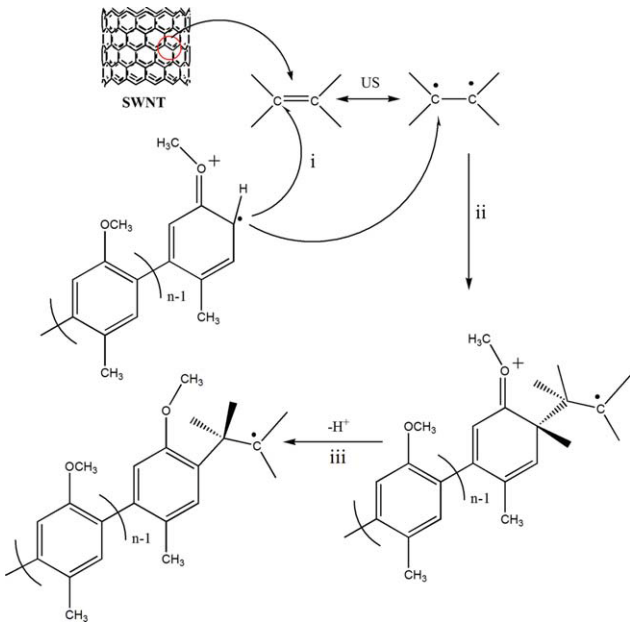

Scheme 2 Schematic grafting mechanism of the oligomer to the SWNTs nanotubes. [Color figure can be viewed in the online issue, which is available at wileyonlinelibrary.com.]

130–200 cm^{-1}) in SWNTs and the composite. Using the inverse relationship between RBM mode frequency and the tube diameter (d) proposed by Rao et al.[52] ($\nu(cm^{-1}) = \frac{223.75}{d(nm)}$), the two bands located at about 144.80 and 160.71 cm^{-1} [Fig. 11(a)], respectively, attributed to the RBM of SWNTs activated in isolated and bundled nanotubes[53] indicate that the resonance Raman occurs at the diameter varying from 1.39 to 1.54 nm. However, taking into account the down-shift due to the oligomer [Fig. 11(b)], it appears that the latter interacts strongly with nanotubes within a 1.47 nm diameter range.

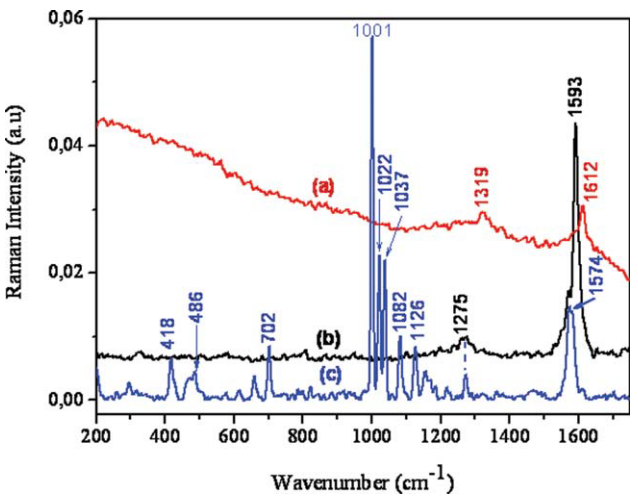

Figure 10 Raman spectra of (a) oligomer, (b) SWNTs, and (c) composite. [Color figure can be viewed in the online issue, which is available at wileyonlinelibrary.com.]

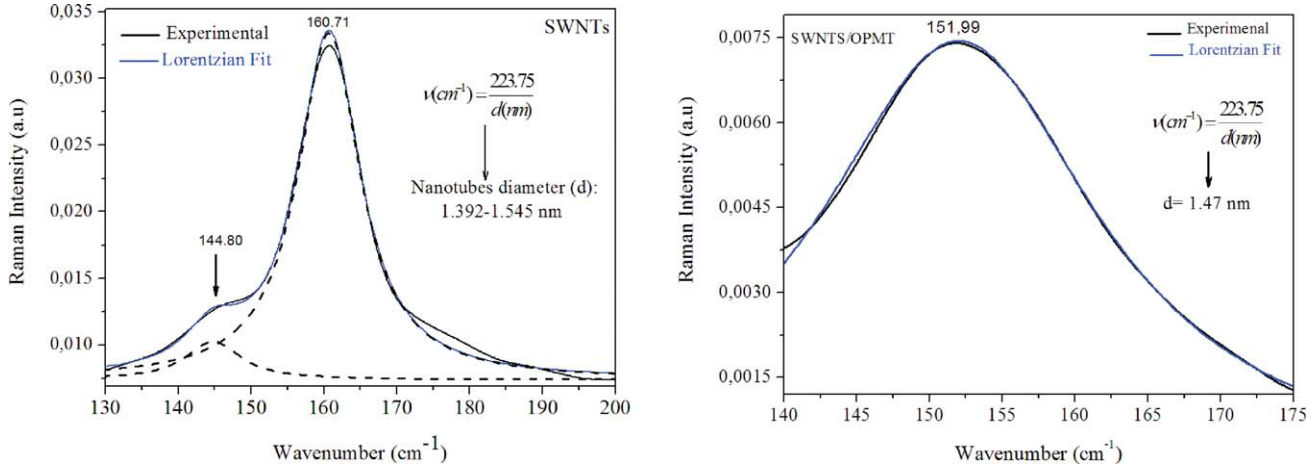

Figure 11 Radial breathing mode features of (a) SWNTs and (b) composite samples. [Color figure can be viewed in the online issue, which is available at wileyonlinelibrary.com.]

CNTs functionalization

To explain the CNTs' oligomer-assisted dispersion and the strong interaction observed by optical measurements, infrared absorption, and Raman scattering changes, a noncovalent functionalization can be suggested. In fact, since it was shown that the OPMT can perform supramolecular π-stacking interactions, this oligomer can probably adsorb on the CNTs surface and facilitate their dispersion in the same way as done by pyrene and its derivatives.[54,55]

Nevertheless, the CNTs dispersion by covalent interactions is not ruled out. It is commonly held that aromatic radicals can bind covalently to atoms of a carbon electrode during diazonium salts reduction.[56] Similarly, CNTs have been recently functionalized.[57] These results substantiated that carbon in graphite, fullerenes, or CNT form is reactive with aromatic radicals. Moreover, grafting methods were recently reported for the covalent bonding of radical polymers onto fullerenes and CNTs.[58–60] In our case, since the oligomer was obtained at a doped state resulting from an overoxidation during the electrochemical synthesis, it will contain stabilized radical cations. The electron delocalization through the polyphenylene backbone will endow the oligomer with a distonic character allowing a free radical-like reactivity. Thereby, the oligomer radical cation can bond to CNTs surface as in the abovementioned cases. This radical reactivity can be enhanced by sonication and cavitation effects, generating very high local temperatures and pressures. A possible schematic grafting mechanism of the oligomer to the SWNTs nanotubes can be evoked (Scheme 2).

Three steps were involved to achieve the grafting mechanism: the first step denoted (i) is the oligomer radical cation attack on a carbon double bond of the CNT or on a radical exited state produced by ultrasound treatment; the second (ii) illustrates the covalent bond establishment between the oligomer and the CNT, and the third (iii) is a proton loss leading to the final functionalized CNT. The generated unpaired electron can be stabilized by delocalization over the CNT skeleton and remains as a structure default or it can react with another oligomer chain in a similar way. Finally, covalent and noncovalent functionalization can be, plausibly, simultaneously involved.

CONCLUSIONS

In this work we have investigated the optical behavior of short-chain oligomer (OPMT) obtained by anodic oxidation of *para*-methoxytoluene. This oligomer is thermally stable up to 242°C. The photoluminescence study reveals the semiconductor character of the studied material. The compound exhibits a tendency to self organize via π-π stacking in solution and solid states. This behavior was evinced by a red-shifted light emission.

When de-doped, the considered oligomer exhibits a well resolved emission signal. This was probably caused by the removal of the intermediate energy levels in the doped state.

Furthermore, this study reveals that OPMT is a good candidate for hosting SWNTs and nanocomposite elaboration. Moreover, the presence of SWNTs causes a clear quenching of light emission and a blue shift of the luminescence peak of the composite, resulting in the shortening of the effective π-conjugation length of the oligomer. Finally, our study shows that the studied oligomer and its SWNTs composite may be good candidates for optoelectronic devices.

References

1. Shirakawa, H.; Louis, E. J.; MacDiarmid, A. G.; Chiang, C. K.; Heeger, A. J. J Chem Soc Chem Commun 1977, 578.

2. Skotheim, T.; Reynolds, J. R.; Elsenbaumer, R. L., Eds.; Handbook of Conducting Polymers; Marcel Dekker: New York, 1997; Vol. II.
3. Heeger, A. J. In: Conjugated Polymers: The Interconnection of Chemical and Electronic Structure; Salaneck, W. R., Lundstrokm, I., Rånby, B. Eds.; Oxford University Press: Oxford, 1993; p 27.
4. Salaneck, W. R.; Clark, D. T.; Samuelsen, E. J. Eds.; Science and Technology of Conducting Polymers; Adam Hilger: Bristol, 1991.
5. Li, X. C.; Sirringhaus, H.; Garnier, F.; Holmes, A. B.; Moratti, S. C.; Feeder, N.; Clegg, W.; Teat, S. J.; Friend, R. H. J Am Soc 1998, 120, 2206.
6. Sirringhaus, H.; Tessler, N.; Friend, R. H. Science 1998, 280, 1741.
7. Ram, M. K.; Sarkar, N.; Bertoncello, P.; Sarkara, A.; Narizzano, R.; Nicolini, C. Synth Met 2001, 122, 369.
8. Halls, J. J. M.; Walsh, C. A.; Greenham, N. C.; Marseglia, E. A.; Friend, R. H.; Moratti, S. C.; Holmes, A. B. Nature 1995, 376, 498.
9. Friend, R. H.; Gymer, R. W.; Holmes, A. B.; Staring, E. G. J.; Marks, R. N.; Taliani, C.; Bradley, D. D. C.; dos Santos, D. A.; Brédas, J. L.; Lokgdlund, M.; Salaneck, W. R. Nature 1998, 397, 121.
10. Gustafsson, G.; Cao, Y.; Treacy, G. M.; Klavetter, F.; Colaneri N.; Heeger, A. J. Nature 1992, 357, 477.
11. Lère-Porte, J.-P.; Moreau, J. J. E.; Torreilles, C. Synth Met 1999, 101, 104.
12. Pron, A.; Rannou, P. Prog Polym Sci 2002, 27, 135.
13. Lu, S.; Fan, Q.-L.; Xiao, Y., Chua, S.-J., Huang, W. Thin Solid Films 2002, 417, 215.
14. Brédas, J. L.; Beljonne, D.; Cornil, J.; Calbert, J. P.; Shuai, Z.; Silbey, R. Synth Met 2001, 125, 107.
15. Klärner, G.; Müller, M.; Morgenroth, F.; Wehmeier, M.; Soczka-Guth, T.; Müllen, K. Synth Met 1997, 84, 297.
16. Bednarz, M.; Reineker, P.; Mena-Osteritz, E.; Bäuerle, P. Chem Phys 2007, 342, 191.
17. Fu, Y.; Shen, W.; Li, M. Polymer 2008, 49, 2614.
18. Chai, S. P.; Zein, S. H. S.; Mohamed, A. R. Diam Rel Mater 2007, 16, 1656.
19. Wang, J.; Lin, Y. Trend Anal Chem 2008, 27, 619.
20. Al-Saleh, M. H.; Sundararaj, U. Polymer 2010, 51, 2740.
21. Paul, D. R.; Robeson, L. M. Polymer 2008, 49, 3187.
22. Zaidi, B.; Bouzayen, N.; Wéry, J.; Alimi, K. J Mol Struct 2010, 971, 71.
23. Song, L.; Zhang, H.; Zhang, Z.; Xie, S. Compos Appl Sci Manufact 2007, 38, 388.
24. Gou, J.; Minaie, B.; Wang, B.; Liang, Z.; Zhang, C. Comput Mater Sci 2004, 31, 225.
25. Zheng, Q.; Xia, D.; Xue, Q.; Yan, K.; Gao, X.; Li, Q. Appl Surf Sci 2009, 255, 3534.
26. Ma, P. C.; Siddiqui, N. A.; Marom, G.; Kim, J. K. Compos Appl Sci Manufact 2010, 41, 1345.
27. Sahoo, N. G.; Rana, S.; Cho, J. W.; Li, L. Chan, S. H. Prog Polym Sci 2010, 35, 837.
28. Said, A. H.; Dridi, C.; Roudesli, S.; Mhalla, F. M. Eur Polym Mater 2000, 36, 909.
29. Zaidi, B.; Bouzayen, N.; Wéry, J.; Alimi, K. Mater Chem Phys 2011, 126, 417.
30. Li, S.; Li, Z.; Fang, X.; Chen, G. Q.; Huang, Y.; Xu, K. J Appl Polym Sci 2008, 110, 2085.
31. Kukovecz, A.; Kramberger, C.; Holzinger, M.; Kuzmany, H.; Schalko, J.; Mannsberger, M; Hirsch, A. J Phys Chem B 2002, 106, 6374.
32. Curtis, M. D. In Proceedings of the 10th Annual Symposium of the NSF Center University of Rochester; World Scientific: Singapore, 2000; p 77.
33. Guillet, J. Polymer Photophysics and Photochemistry: An Introduction to the Study of Photo Process in Macromolecules; Cambridge University Press: New York, 1987; p 141.
34. Chapuzet, J. M.; Simonet, J. Tetrahedron 1991, 47, 791.
35. Gebauer, W.; Väterlein, C.; Soukopp, A.; Sokolowwski, M.; Hock, R.; Port, H.; Päuerle, P.; Umbach, E. Synth Met 1997, 87, 127.
36. Mulazzi, E.; Ripamonti, A.; Wéry, J.; Dulieu, B.; Lefrant, S. Phys Rev B 1999, 60, 16519.
37. Aarab, H.; Baitoul, M.; Wéry, J.; Almairac, R; Lefrant, S.; Faulques, E.; Duvail, J. L.; Hamedoun, M. Synth Met 2005, 155, 63.
38. Mulazzi, E.; Botta, C.; Facchinetti, D.; Bolognesi, A. Synth Met 2004, 142, 85.
39. Kymakis, E.; Amaratunga, G. A. J Appl Phys Lett 2002, 80, 112.
40. Kymakis, E.; Alexandou, I.; Amaratunga, G. A. J Synth Met 2002, 127, 59.
41. Yang, Y.; Pei, Q.; Heeger, A. J Synth Met 1996, 78, 263.
42. Lefrant, S.; Baibarac, M.; Baltog, I.; Godon, C.; Mevellec, J. Y.; Wéry, J.; Faulques, E.; Mihut, L.; Aarab, H.; Chauvet, O. Synth Met 2005, 155, 666.
43. Kim, U. J.; Liu, X. M.; Furtado, C. A.; Chen, G.; Saito, R.; Jiang, J.; Dresselhaus, M. S.; Eklund, P. C. Phys Rev Lett 2005, 95, 157402.
44. Rasheed, A.; Chae, H. G.; Kumar, S.; Dadmun, M. D. Polymer 2006, 47, 4734.
45. Rao, C. N. R. Chemical Application of Infrared Spectroscopy; Academic Press: New York, 1963; p 156.
46. Mayo, D. M.; Miller, F. A.; Robert, W. H. Course Notes on the Interpretation of Infrared and Raman Spectra, 1st ed.; John Wiley: Hoboken, NJ, 2004; p 101.
47. Pham, M. C.; Aeiyach, S.; Moslih, J.; Soubiran, L.; Lacaze, P. C. J Electro Chem 1990, 277, 327.
48. Said, A. H.; Mhalla, F. M.; Amatore, C.; Verpeaux, J. N. J Electroanal Chem 1999, 464, 85.
49. Piscanec, S.; Lazzeri, M.; Robertson, J.; Ferrari, A. C.; Mauri, F. Phys Rev B 2007, 75, 035427.
50. Claye, A.; Rahman, S.; Fischer, J. E.; Sirenko, A.; Sumanasekera, G. U.; Eklund, P. C. Chem Phys Lett 2001, 333, 16.
51. Bendiab, N.; Anglaret, E.; Bantignies, J.-L.; Zahab, A.; Sauvajol, J. L.; Petit, P.; Mathis, C.; Lefrant, S. Phys Rev B 2001, 64, 245424.
52. Rao, A. M.; Richter, E.; Bandow, S.; Chase, B.; Eklund, P. C.; Williams, K. A.; Fang, S.; Subaswamy, K.; Menon, M.; Thess, A.; Smalley, R. E.; Dresslhaus, G. Science 1997, 275, 187.
53. Luo, Z.; Li, R.; Kim, S. N.; Papadimitrakopoulos, F. Phys Rev B 2004, 70, 245429.
54. Yan, Y.; Cui, J.; Pötschke, P.; Voit, B. Carbon 2010, 48, 2603.
55. Delamar, M.; Hitmi, R.; Pinson, J.; Savéant, J. M. J Am Chem Soc 1992, 114, 5883.
56. Bourdillon, C.; Delamar, M.; Demaille, C.; Hitmi, R.; Moiroux, J.; Pinson, J. J Electroanal Chem 1992, 336, 113.
57. Bahr, J. L.; Yang, J.; Kosynkin, D. V.; Bronikowski, M. J.; Smalley, R. E.; Tour, J. M. J Am Chem Soc 2001, 123, 6536.
58. Okamura, H.; Terauchi, T.; Minoda, M.; Fukuda, T.; Komatsu, K. Macromolecules 1997, 30, 5279.
59. Lou, X.; Detrembleur, C.; Sciannamea, V.; Pagnoulle, C.; Jérôme, R. Polymer 2004, 45, 6097.
60. Homenick, C. M.; Lawson; G.; Adronov, A. Polym Rev 2007, 47, 265.